SUPPLEMENTARY INFORMATION

Thermally switchable nanogate based on polymer phase transition

Pauline J. Kolbeck[1,2,3*], Dihia Benaoudia[4,5*], Léa Chazot-Franguiadakis[1], Gwendoline Delecourt[5], Jérôme Mathé[6], Sha Li[6], Romeo Bonnet[4], Pascal Martin[4], Jan Lipfert[2,3], Anna Salvetti[7], Mordjane Boukhet[8], Véronique Bennevault[5,9], Jean-Christophe Lacroix[4], Philippe Guégan[5], Fabien Montel[1†]

Affiliations:

1: Univ Lyon, ENS de Lyon, CNRS, Laboratoire de Physique, F-69342 Lyon, France

2: Department of Physics and Center for NanoScience, LMU Munich, 80799 Munich, Germany

3: Department of Physics and Debye Institute for Nanomaterials Science, Utrecht University, 3584 CC Utrecht, The Netherlands

4: Université Paris Cité, ITODYS, CNRS, F-75006 Paris, France

5: Institut Parisien de Chimie Moléculaire, *Equipe Chimie des Polymères,* UMR CNRS 8232, Sorbonne Université, Paris 75252, France

6: Université Paris-Saclay, Univ Evry, CNRS, LAMBE, Evry-Courcouronnes, France

7: Centre International de Recherche en Infectiologie, INSERM U111, UMR CNRS 5308, Université Claude Bernard Lyon 1, Lyon 69007, France

8: Center for Molecular Bioengineering (B CUBE), Technical University of Dresden, Dresden, Germany

9: University of Evry, Evry 91000, France

*Contributed equally to this work
† Corresponding Author Fabien Montel. Email: fabien.montel@ens-lyon.fr

SUPPLEMENTARY MATERIALS AND METHODS

Experimental setup

Our experimental setup combines optical detection and pressure control to induce the transport of polymers through a porous membrane as previously described by Auger *et al.* (1, 2) (**Figure 1**). Briefly, the experimental setup is based on an inverted fluorescence microscope (Axiovert 200) with a filter box – including several pairs of excitation and emission filters and an associated dichroic mirror – connected to an electron-multiplying charge-coupled device camera (EMCCD camera, Andor, iXon 897). When imaging directly, it shows a maximum resolution of 512 x 512 pixels in 32 bits and a maximum frame rate of 60 Hz. A water objective (ZEISS C-Apochromat) with 63x magnification, 1.2 numerical aperture, and 0.28 mm operating distance for a 0.17 mm glass slide is mounted on the microscope. We use a laser (Cobolt blues 50, Cobolt AB), which emits at 473 nm wavelength, as excitation source. The beam is expanded by a telescope and parallelized inside the optical path. The membrane is illuminated from the trans side. The setup has a second light source, a fluorescent lamp (Uvico, Optoelectronics GmbH), directly connected to the microscope via an optical fiber. The two possible excitation wavelengths are 488 nm and 568 nm. The lamp is used to get a better overview of the sample and to light the sample with or without heating, depending on the selected excitation wavelength. The centerpiece of the setup is composed of two chambers separated by a porous membrane: the upper chamber (called the *cis* chamber) consists of a screw cap (Nanion) made of a glass bottom with a small hole on which a piece of membrane is glued. This chamber is linked to a pressure control system (MFCS, Fluigent) that allows the application of pressures up to 1 bar with a precision better than 0.1 mbar. Sealing is accomplished by a Teflon gasket inside the cap. The lower chamber also called *trans* chamber, is made of a Teflon ring on which a 0.17 mm thick glass strip is attached. In addition, the setup has a smaller Teflon ring fitted around the screw cap to maintain it vertically in the *trans* chamber. The translocated polymer – labeled with a fluorescent dye - is introduced into the *cis* chamber, and by applying a pressure difference between the two chambers, the polymer is translocated through the membrane into the *trans* chamber. As the membrane is illuminated with an extended laser beam on the *trans* side, on which the gold coating is grafted, the molecules can be observed leaving the pores. In contrast, molecules in the *cis* chamber and inside the pore are dark since they are not within the illuminated volume. Finally, the fluorescence of the molecules vanishes due to bleaching and optical defocusing once they move away from the membrane. This two-chamber construction is located above the lens of the fluorescence microscope. The sample can be moved in all three directions by a stage control system with an XY-drive with µm-accuracy and a Z-drive with nm-accuracy. The stage control system is operated by the software ImageJ. The transported molecules are observed by an operating software (Andor SOLIS for imaging) that is connected to the EMCDD camera.

Membrane preparation and polymer grafting

We pretreated the nanoporous membranes, again following the protocol of Auger *et al*. (1, 2). The commercially available track-etched membranes (Whatman) consist of a 6-10 µm-thick polycarbonate layer and have cylindric holes (pores) with a nominal diameter of 50 or 200 nm and a density of $1\text{-}6.10^8$ pores/cm^2. To visualize the translocation of molecules through the pores, we vapor deposited a gold layer of 50 nm thickness after a pre-treatment of low-intensity

ionic pickling. Gold was evaporated, using a pressure below 10^{-6} Pa, and deposited at a rate of 0.2 nm/s. The rate and thickness of the deposition were monitored by a quartz balance.

The polymer grafting (**Table 1**) on top of the gold layer used electro-grafting, i.e connection between the polymers and the gold surface via covalent bounds generated by diazonium salt reduction (3, 4). Polymers used in this article were poly(2-methyl-2-oxazoline)s (PMeOx) and poly(2-*n*-propyl-2-oxazoline)s (P*n*PrOx) of various number-average degrees of polymerization (X_n, number of repeat units).

In the next step, a covalent bond between the polymer and the gold surface was formed by reduction of the diazonium salt. A detailed protocol for polymer synthesis and electro-grafting can be found in Supplementary Information **S1** and **S2**.

Sample preparation

For all experiments, we used a tris(hydroxymethyl)aminomethane (Tris) and ethylenediaminetetraacetic acid (EDTA) based buffer (TE buffer), made from Tris-HCl (Sigma-Aldrich) and EDTA (Sigma-Aldrich), pH 7.5. We used Lambda-DNA (Invitrogen) which is a double-stranded linear DNA from bacteriophage λ, (Escherichia coli) consisting of 48,502 base pairs (32,300 kDa). This DNA is commercially available as a solution of 500 µg/ mL in 10 mM Tris-HCl and 1 mM EDTA . The diameter of the DNA molecules is about 2 nm while the contour length (maximum length of the molecule) is about 16 µm. The DNA molecules were fluorescently labeled with YOYO-1 (Life Tech).

For the stationary heating experiments, we introduced 100 µl TE buffer mixed with 2 µl DNA-YOYO mix in the *cis* chamber and 500 µl TE buffer in the *trans* chamber.

As a model of the viral capsid, we used capsids from Adeno-Associated Virus serotype 8 (AAV-8). More precisely, recombinant AAV-8 capsids were produced and purified as described previously (5). Briefly, HEK-293 cells were co-transfected with a helper plasmid (pDG8), containing both rep2-cap8 and the adenoviral helper genes, and the AAV2-CMV-GFP vector plasmid (encoding for GFP under the control of the cytomegalovirus (CMV) promoter). Particles were purified from cell lysates on a double CsCl gradient and dialyzed. The concentration of the final AAV-8 sample was determined using qPCR and was equal to 1.4×10^{12}vg/mL.
Fluorescent labeling was achieved using YOYO-1 which was diluted 1500 in the AAV-8 solution (labeling required incubation for 10 min at room temperature). Serum Fetal Bovin (FSB) was added to 10% of the final virus solution.

DNA or virus samples were placed in the *cis* chamber. To apply specific temperatures, we made use of a temperature control system (Pecon, TempController 2000-2). This system allows us to heat a metal ring that is located around the objective. As the objective is connected by a drop of water to the *trans* chamber which in turn is filled with buffer that is in contact with the membrane, we have the possibility to indirectly heat the membrane. The applied temperature at the level of the heater was chosen to be 50 °C. After the temperature control system had reached this temperature, we waited for 60 minutes to make sure that the whole system is heated up to sufficiently high temperature. The temperature of the buffer in the *trans* chamber was checked to be higher than 30 °C using a thermometer with a long and flexible probe that is placed on the side of the inner edge of the *trans* chamber so that it is in contact with the liquid inside.

Thereafter, we switched off the heat supply and let the system cool down while taking one video every minute. With the acquisition of a video, we also measured and noted the temperature of the liquid in the *trans* chamber.

For varying pressure experiments, we introduced 100 µl TE buffer mixed with 2 µl DNA-YOYO mix in the *cis* chamber and 500 µl TE buffer in the *trans* chamber. The applied pressure was changed between 0 mbar and 150 mbar using the pressure control system. After setting a pressure value at the control system, we waited 3 minutes to let the system adapt. Then, we took four videos in a row at constant pressure. The measurements were either performed at room temperature or while heating the system as explained for the stationary heating experiment.

Data analysis

To determine the translocation frequency, the single-molecule translocation events appearing in the video are counted manually. Translocation events are visible as bright spots on the otherwise dark background (the membrane is only slightly auto-fluorescent). The frequency *f* is then calculated as the number of events *N* observed during one video sequence divided by the number of pores present in one film N_P times the acquisition time $t_{acq} = 15\ s$. N_P can be calculated as the pore density ρ = 6-10.10^8 pores/cm^2 times the observed area 150 µm x 150 µm:

$$f = \frac{N}{N_p t_{acq}} = \frac{N}{\rho A t_{acq}} \quad (1)$$

Further data analysis was carried out using custom MATLAB routines. For the analysis of the stationary heating experiments, we plotted the number of translocation events as a function of time and the measured temperature. As the temperature was taken at the edge of the *trans* chamber, the noted temperature differs from the actual temperature of the membrane, but we assumed that these two temperatures are not far from each other. The resulting curves were normalized by setting the starting frequency value to one. Subsequently, the temperature-frequency curves were fitted by an error function defined as:

$$erf(x) = \frac{2}{\sqrt{\pi}} \int_0^x e^{-t^2} dt \quad (2)$$

We note that the use of an error function is not motivated by a specific physical model, but just provides a convenient expression to provide an accurate mathematical fit.

For varying pressure experiments, we took the mean value of the number of translocation events of the four videos recorded at the same pressure. This value was then represented as a function of the applied pressure and fitted using the suction model (3). In this theoretical framework, the frequency of translocation *f* can be written as

$$f = k \cdot (P / P_c) \cdot \exp(-P_c / P) \quad (3)$$

with *k* being constant, *P* the applied pressure, and P_c the critical pressure. By fitting this equation to our data points, we were able to obtain values for *k* and P_c. Here, we were mainly interested in P_c, the minimum pressure that is required to transport the molecule through the pore.

SUPPLEMENTARY FIGURES, TABLES, AND NOTES

S1: Polymer synthesis and characterization of synthesized polymers

The polymerization of 2-alkyl-2-oxazolines was accomplished through a process of Cationic Ring Opening Polymerization (CROP), which was well-controlled (6, 7). Polymer's structure and the reaction recap are represented in Figure S1-1. Polymers used in this article were poly(2-methyl-2-oxazoline)s (PMeOx) and poly(2-*n*-propyl-2-oxazoline)s (P*n*PrOx).

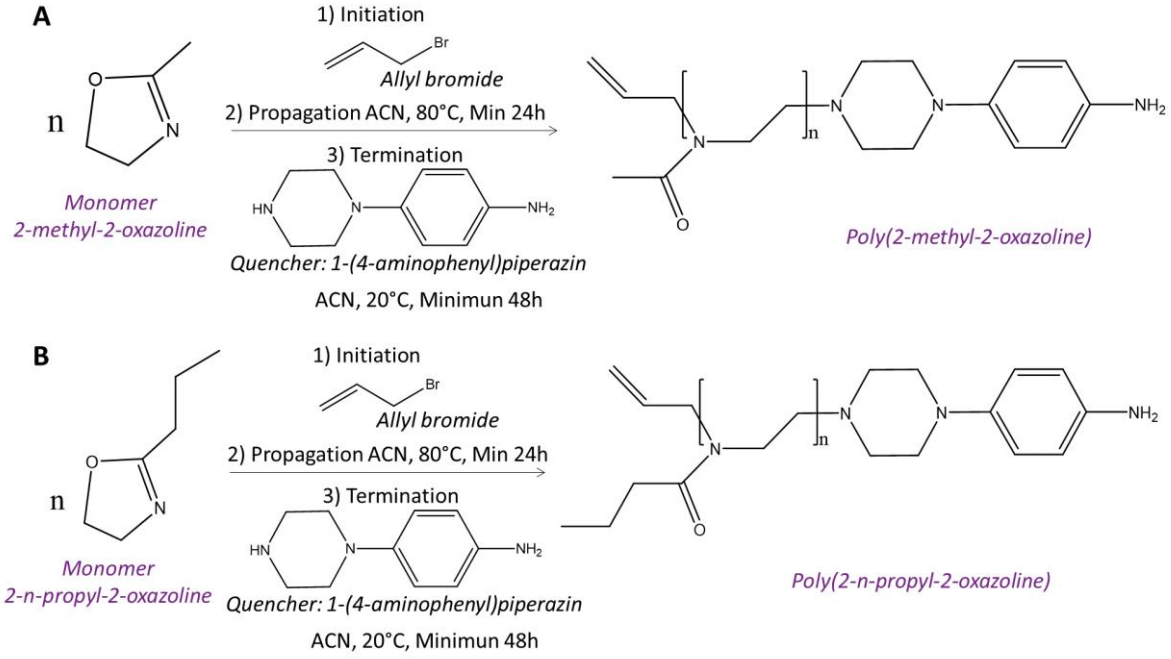

Figure S1-1: **Balance equation for the polymerization reaction** of A) PMeOx and B) P*n*PrOx.

A description of the chemical mechanism for the PMeOx polymerization is also depicted in Figure S1-2. The mechanism is similar for the P*n*PrOx polymerization since only the structure of the monomer changes (see Figure S1-1).

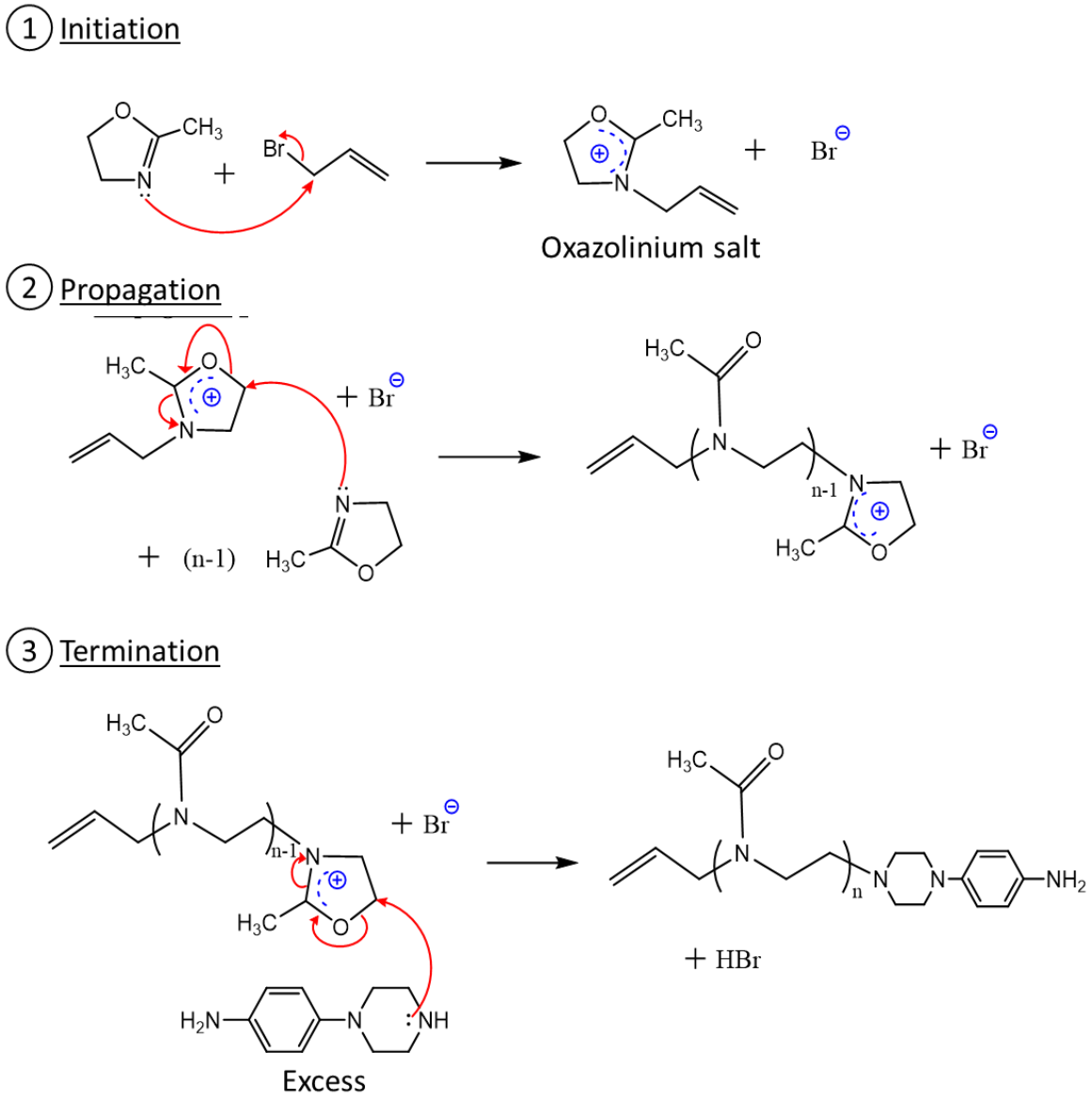

Figure S1-2: **Polymerization mechanism for PMeOx (Cationic Ring Opening Polymerization, ionic mechanism)**. (1) Initiation: it consists in the nucleophilic attack of the non-bonding doublet of the nitrogen atom of the monomer on the electrophilic site of the initiator and generates an oxazolinium salt. (2) Propagation: the oxazolinium salt undergoes a nucleophilic attack of the monomer. This attack is done on carbon 5, which induces the opening of the ring. (3) Termination: it is based on the addition of the deactivating agent (1-(4-aminophenyl)piperazine). The nucleophilic part (aniline side) attacks the carbon 5, which generates polymer chains whose active center is deactivated.

Polymer synthesis

Polymers used in this article were PMeOx and P*n*PrOx of various polymerization degrees (X_n). The polymerization of 2-alkyl-2-oxazolines was well-controlled. The reagents of the polymerization were:

-Initiator: Allyl bromide (AlBr, 99%, *Sigma Aldrich*)

-Monomers: 2-methyl-2-oxazoline (98%, *Sigma Aldrich*), 2-*n*-propyl-2-oxazoline (97%, *TCI*)

-Terminating agent: 1-(4-aminophenyl)piperazine (97%, *Sigma Aldrich*). It was chosen in order to introduce an aminophenyl group at the end of the polymer chain.

Those reagents and the solvent (acetonitrile, ACN, *Sigma Aldrich*) were first cryo-distilled over calcium hydride to remove any trace of water. The reaction was carried out in ACN at 80°C under inert atmosphere. The reagents were introduced in the following order: initiator, ACN, and then the monomer. After a variable time (depending on the expected degree of polymerization), the terminating agent in solution in DMF was introduced in the reaction medium in excess. The polymers were then dialyzed using a regenerated cellulose membrane (Repligen, Spectra/Pore 6, Standard Regenerated Cellulose, cut-off 1000 Da) against methanol.

Polymer characterization

The polymers were characterized using ^{1}H NMR (Bruker Nanobay 300 MHz, in $CDCl_3$ solvent) and Size Exclusion Chromatography (SEC, in N,N-dimethylformamide, with poly(methyl methacrylate) standards).

^{1}H NMR

The spectrometer used was the Bruker Nanobay 300 MHz. The solutions of polymers were prepared at 30 mg/mL with $CDCl_3$ (Euriso-TOP). The spectra were processed with the MestReNova software. The calibration of the spectrum was performed with the signal of the solvent here of $CDCl_3$, which appears as a singlet at 7.26 ppm. The attribution of the protons and their chemical displacement were shown for two examples in the Figure S1-3: PMeOx (X_n= 387) and P*n*PrOx (X_n=538).

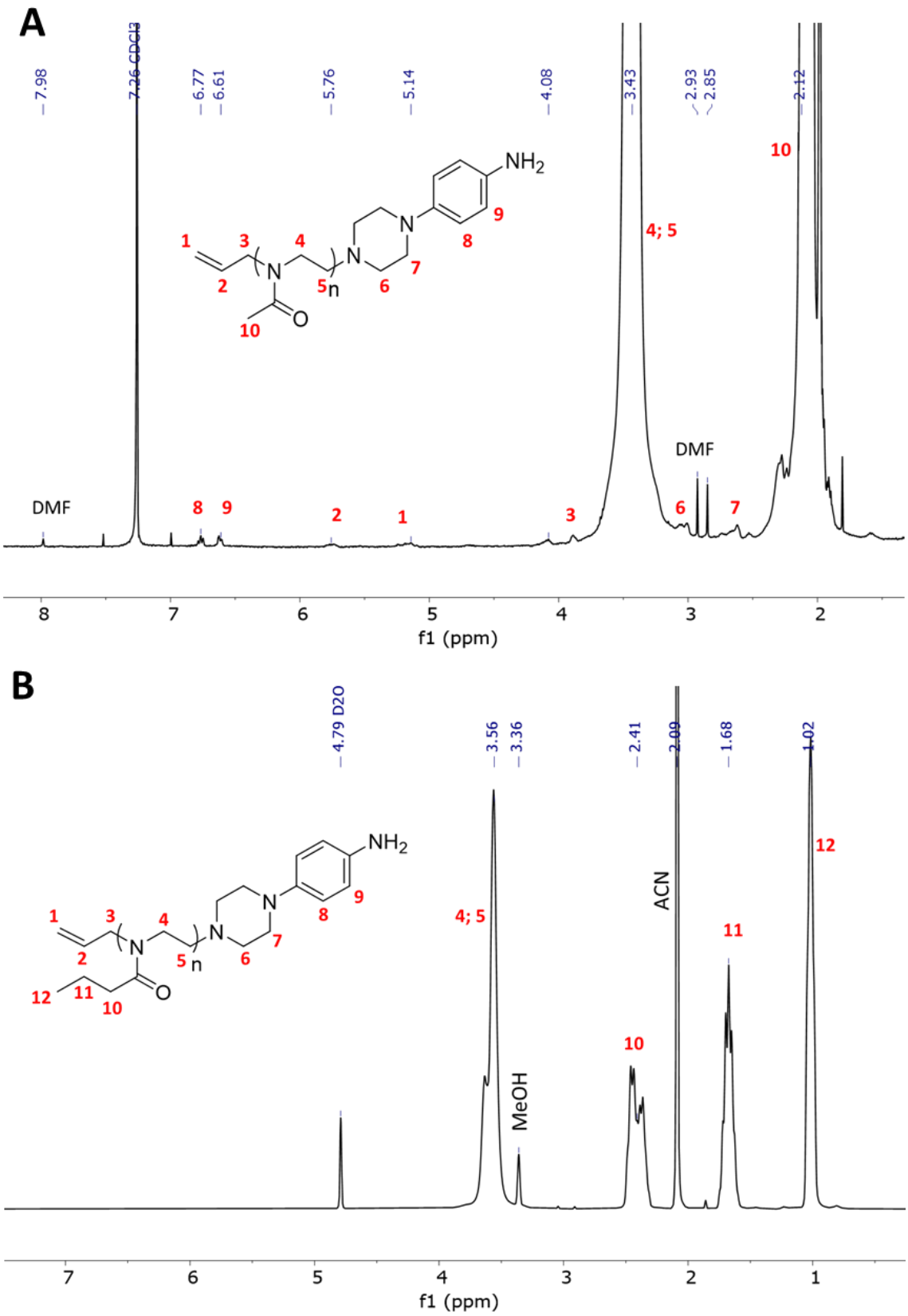

Figure S1-3: **^{1}H NMR** of A) PMeOx (X_n=387) and B) P*n*PrOx (X_n=538). The assignment of the protons was given in red and their chemical displacement in blue.

Steric Exclusion Chromatography, SEC

The mobile phase used was N,N-dimethylformamide (DMF, Sigma Aldrich) at 60 °C and the SEC was performed with a PSS GRAM 100 nm (8×300 mm; separation limits: 1 to 1000 kg.mol-1) coupled to a differential refractive index (RI) detector. The degree of polymerization (X_n) and the dispersity (Đ) of the polymers were calculated using calibration standards in PMMA (polymethylmethacrylate). Examples of SEC chromatograms for PMeOx (X_n=387) and P*n*PrOx (X_n=538) were given in Figure S1-4.

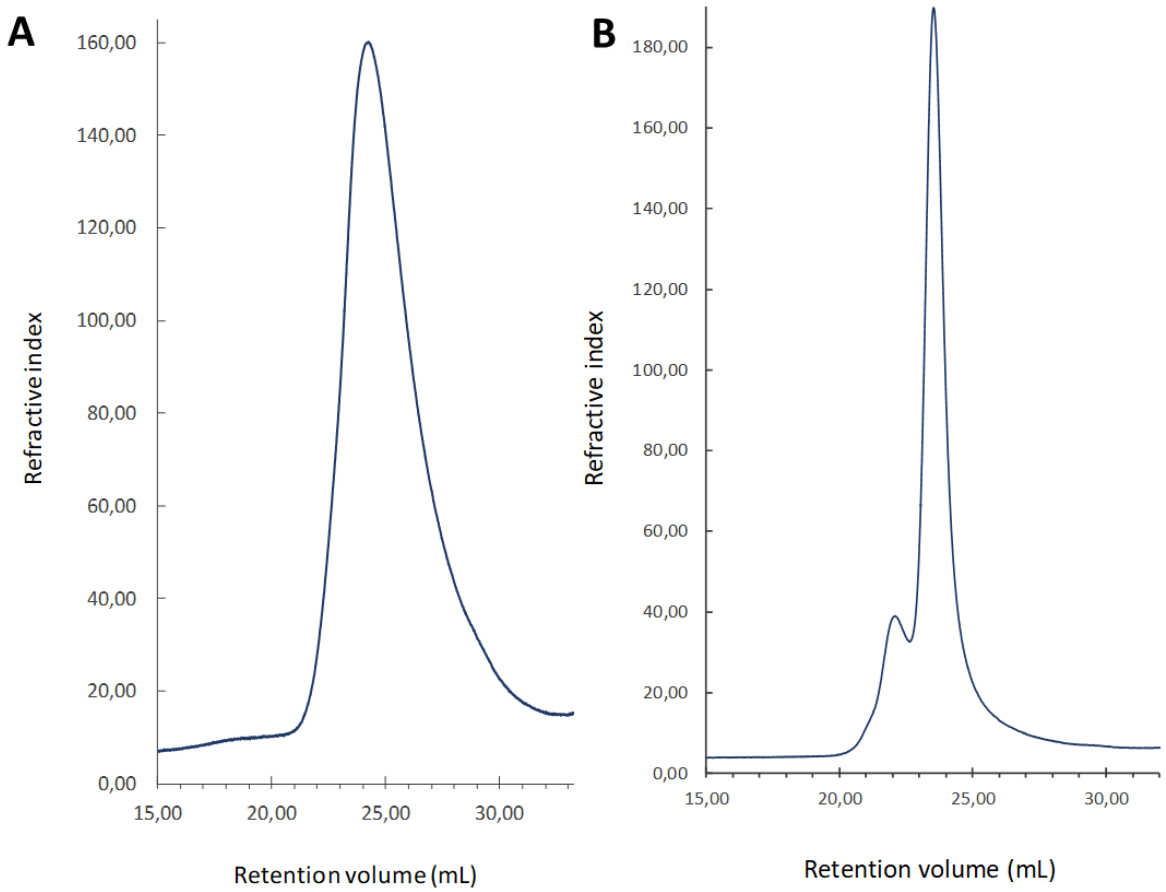

Figure S1-4: **Chromatograms** of A) PMeOx (X_n= 387) and B) P*n*PrOx (X_n=538).

The final degree of polymerization (X_n) was obtained by averaging the polymerization degree from the data of ^{1}H NMR and the data from SEC. The results are presented in Table S1-1 and S1-2, respectively for PMeOx and P*n*PrOx.

Table S1-1: **Characterization of PMeOx**

X_n (theory) [a]	X_n (NMR)[b]	X_n (SEC)[c]	X_n **(average)**[d]	Đ [c]
54	57	64	**61**	1.30
59	81	85	**83**	1.35
176	174	182	**178**	1.38
530	-	387	**387**	1.71

[a] $X_n = ([MeOx]_0 \times \rho_{MeOx}) / [AlBr]_0$ with ρ_{MeOx} corresponding to MeOx conversion
[b] determined by ^{1}H NMR from signals of allyl protons and methylene protons from the polymer backbone
[c] Đ corresponds to polymer dispersity determined by SEC in DMF, PMMA standards
[d] average between NMR and SEC values

Table S1-2: **Characterization of P*n*PrOx**

X_n (theory) [a]	X_n (NMR)[b]	X_n (SEC [c]	X_n **(average)** [d]	Đ[c]
39	32	34	**33**	1.12
30	51	64	**59**	1.08
176	226	194	**210**	1.2
530	-	538	**538**	1.31

[a] $X_n = ([n\text{PrOx}]_0 \times \rho_{n\text{PrOx}}) / [AlBr]_0$ with $\rho_{n\text{PrOx}}$ corresponding to *n*PrOx conversion
[b] determined by ^{1}H NMR from signals of allyl protons and methylene protons from the polymer backbone
[c]) Đ corresponds to polymer dispersity determined by SEC in DMF, PMMA standards
[d] average between NMR and SEC values

S2: Electrochemical grafting protocol

First, a diazonium salt was generated *in situ* from the aminophenyl end of the polymers in the presence of an acid ($HClO_4$) and a nitrite compound ($NaNO_2$) (3). Then, the formation of a covalent bond between the polymer and the gold surface was achieved by reduction of the diazonium salt. Grafting was accomplished by cyclic voltammetry, scanning the membrane between 0 and -0.8 V/$E_{Ag+/Ag}$ at a scan rate of 0.1 V/s. Several cycles were performed (10 to 20 depending on the membranes).

Grafting characterization

Voltammograms

We used a probe with an external sphere probe that is sensitive to surface states: ferrocenemethanol (FcMeOH). The membranes were characterized before and after grafting. For this purpose, an aqueous solution containing 1 mM of FcMeOH, and 0.1 M of lithium perchlorate (LiClO4, acting as electrolyte) was prepared. The solution was added to the electrochemical cell, and after degassing under Argon for about ten minutes, a first voltammogram before grafting was recorded (scan rate 0.1 V/EAg). After grafting, the same mother solution of FcMeOH is used, following an identical process to characterize the surface. Examples of voltammograms are given in Figure S2-1.

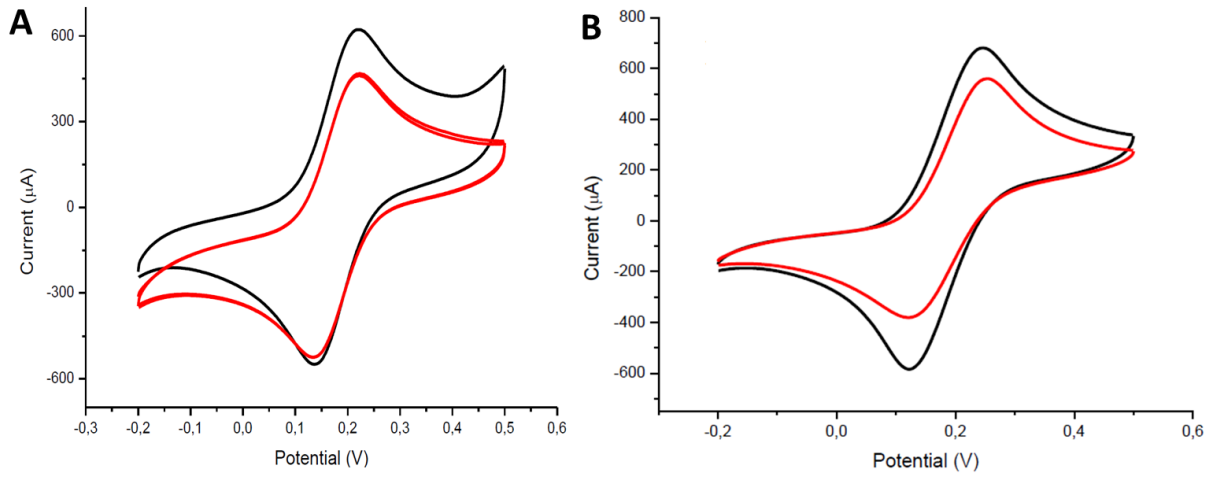

Figure S2-1: **Voltammograms with FcMeOH before (black) and after (red) grafting for a gold nanoporous surface (pores 50 nm) grafted** with A) PMeOx (X_n=61) and B) P*n*PrOx (X_n=33).

The evolution of the voltammogram before and after grafting allows to conclude qualitatively that there was indeed a modification of the surface after grafting.

X-Ray photoelectron spectrometry

XPS relies on the photoelectric effect and allows to measure elemental composition within the surface of a material. The analysis of XPS spectra allow to obtain the percentage of each element on the surface studied. Here we calculate the ratio N/O, C/O, CN and C/Au to evidence the presence of the grafting.

An example of XPS surface from a nanoporous gold membrane (pores of 50 nm in diameter) and grafted with PMeOx (X_n=178) is given in Figure S2-2.

A

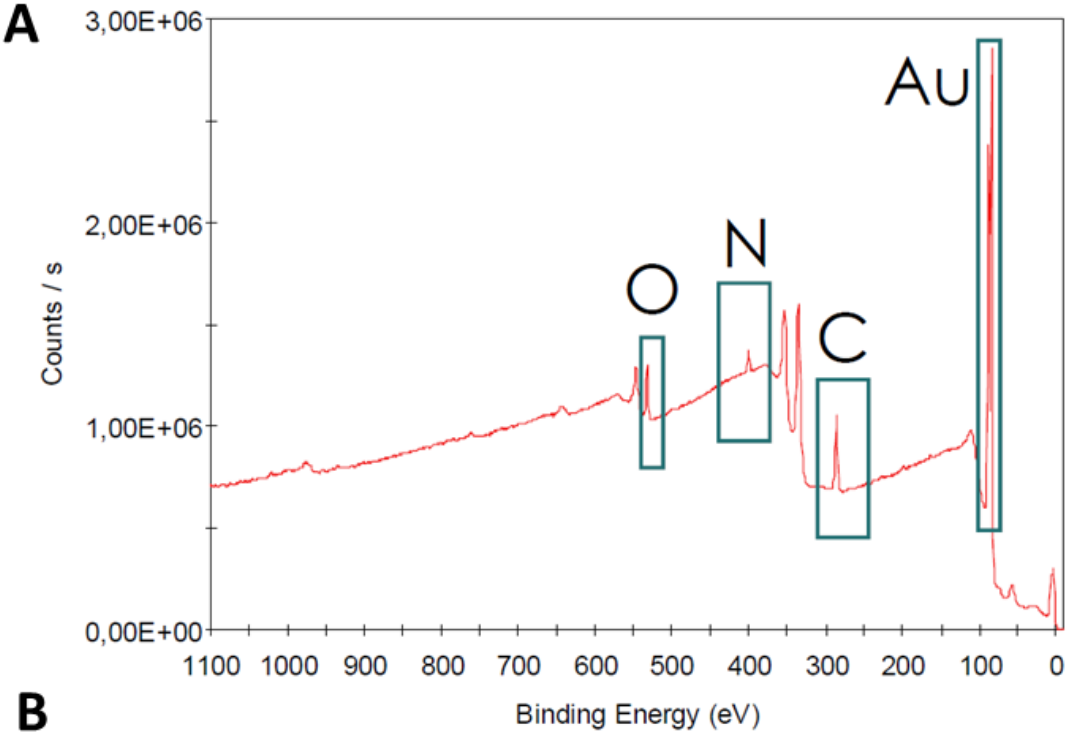

B

Ratio	C/N	C/O	N/O	C/Au
Theory (monomer MeOx)	4	4	1	/
Experimental data	5.9	4.0	0.7	7.0

Figure S2-2: **XPS for a nanoporous gold surface (Pores 50nm in diameter) grafted with PMeOx (X_n=178)** A) Spectrum B) Data analysis.

The results obtained by XPS allow to validate the presence of a grafting. To go further and observe the grafted membranes, measurements were also realized by AFM in liquid medium (see section S9).

S3: Combined illumination and heating using a fluorescence lamp

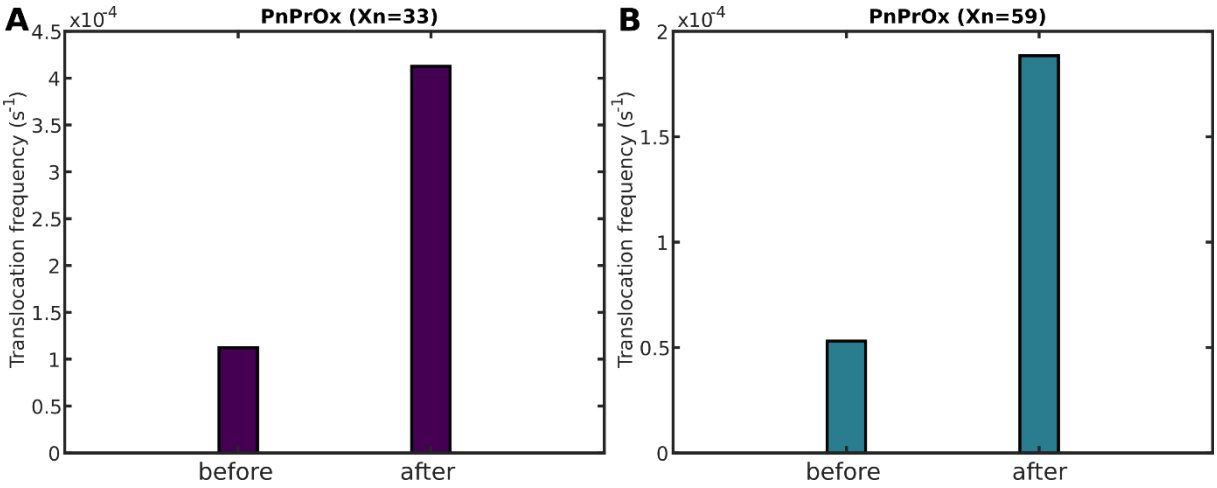

<u>Figure S3</u>: Comparison between the averaged translocation frequency before and after local heating. Using a fluorescent lamp, we were able to heat the membrane sufficiently locally to open the nanopores and allow transport. We exposed the surface of the membrane visible to the camera to the light source only briefly (2 min), which is already enough to exceed the *LCST* when we start the experiment at room temperature (20 °C). The translocation frequency was measured before illumination (label 'before') and after illumination by the fluorescent lamp (label 'after'). In all cases, the illumination is off during the frequency measurement. For both the P*n*PrOx (X_n=33) grafting (A) and the P*n*PrOx (X_n=59) grafting (B), the translocation frequency is increased by about 440 %.

A precise determination of the temperature of the membrane during the heating by the fluorescence lamp is difficult in our system, but we can propose a rough estimate from the parameters of our illumination. At steady state our lamp delivers a power density of ~0.5mW/nm on the membrane. The gold film adsorption in the range of wavelength used in this study is 50% on a 10 nm interval around the plasmon resonance. If we assume that the polycarbonate membrane plays the role of a perfect insulator and that the thermal relaxation is due to thermal conduction through the water we obtain that the temperature change of gold during heating would be in the range of $\Delta T = \frac{\Delta x.q}{k}$. With k=0.6 W/m, the thermal conductivity of water, Δx=100µm the gradient length, q~5 mW the incident power, we obtained ΔT~42 °C. This order of magnitude is in good agreement with the fact that optical illumination enable to cross the critical transition.

S4: Normalized and averaged translocation frequencies

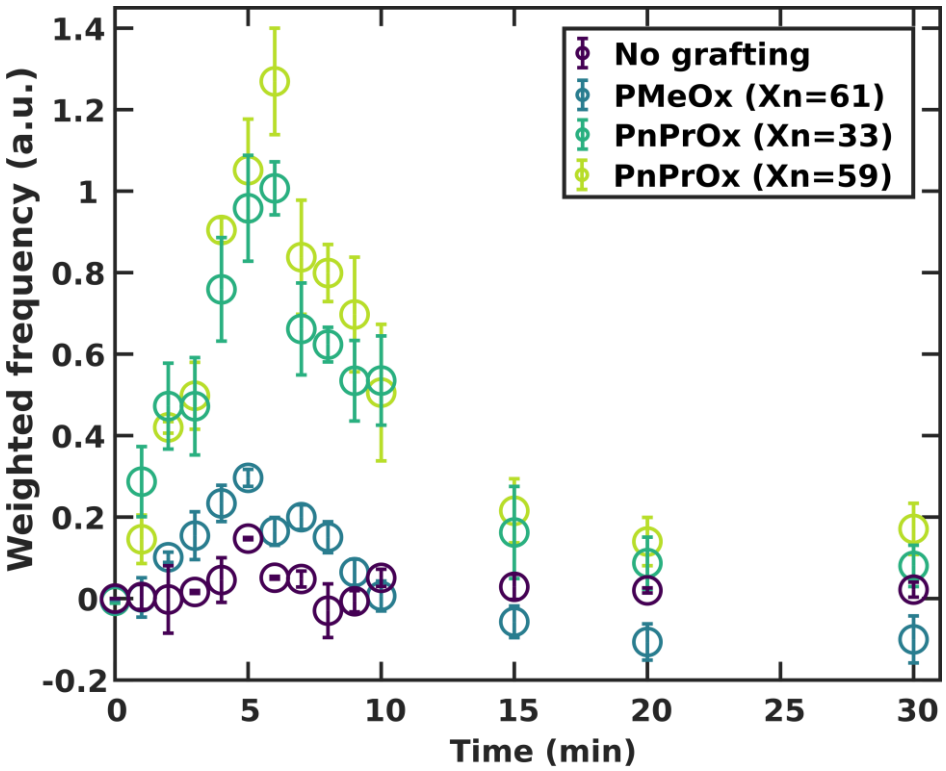

Figure S4: Normalized and averaged translocation frequency as a function of time after heating the system for differently grafted pores. At t=0 the system is shortly heated by inserting high-temperature buffer (70 °C) into the *trans* chamber. This leads to an increase in temperature of the system which in turn increases the translocation frequency; after ~5 minutes, the system relaxes back to room temperature and the translocation frequency decreases again as a result. We normalized and weighted the translocation frequency by the increase between starting frequency and maximum frequency. Polymer grafting: no polymer grafting (purple), PMeOx X_n=61 (blue), P*n*PrOx X_n=33 (dark green), P*n*PrOx X_n=59 (light green).

S5: Theoretical description of the gating phenomenon

Our theoretical description of the gating phenomenon is based on the work of Halperin *et al*.(8) on grafted polymer chain collapse in poor solvent and the suction model. The general idea of this theoretical procedure is to determine the radius of the polymer coil and use it to determine the translocation frequency.

The configuration of the grafted chains is modeled by a mean field theory. We define N as the number of monomer units per chain, R as the polymer coil radius, and a the monomer unit size. We consider the free energy F as composed of two main contributions: F_{el} that accounts for the elongational entropy of the chains and F_{mix} that accounts for the interaction of the monomer

units with the solvent and with the other monomer units. In this case, Halperin *et al.* have shown

$$F = F_{el} + F_{mix}$$

that:

$$F_{el} / k_B T = \alpha^2 - \log(\alpha)$$

$$F_{mix} / k_B T = \int_{coil} c + \frac{1}{2} v a^3 c^2 + \frac{1}{6} w a^6 c^3$$

where $\alpha = R/R_0$ is the expansion factor, R is the coil radius of the grafted polymer, R_0 is the radius of the ideal coil (i.e., in theta solvent), c is the monomer units concentration, v is the second virial coefficient and w is the third virial coefficient.

In our case where the polymer exhibits a lower critical solubility temperature (*LCST*), the second virial coefficient v is negative for low temperature and positive for high temperature, i.e. it changes sign at the theta temperature. In the vicinity of θ, the *LCST*, v may be written as:

$$v = v_0 \cdot \frac{\theta - T}{\theta}$$

In the range of temperatures considered here, the third virial w can be considered to be constant and positive.

We consider the regime where the chains are grafted in the mushroom regime. In this case, D the grafting distance between to polymer is larger than the coil radius ($D > R$). We obtain after integration of F_{mix} on the volume of the coil:

$$F / k_B T = N + v N^{1/2} \alpha^{-3} + w \alpha^{-6} + \alpha^2 - log(\alpha)$$

In order to determine the equilibrium configuration, F is then minimized numerically and the corresponding α^* is measured. The effective radius of the pore R_{eff} is then given by: $R_{eff} = R_{pore} - \alpha^* R_0$ with R_{pore} the pore radius without grafting.

The frequency of translocation can then be determined with the suction model (9). In this model, the energy landscape for a tongue of a flexible polymer subjected to flow injection into the pore. It concludes that a critical flow $J_c = k_B T/\eta$ is sufficient to induce the translocation of any given polymer in any nanopore. This flow is determined by the energy balance between the confinement of the polymer necessary to enter into the pore and the driving force induced by the flow of solvent that creates a drag force on the monomers. This critical phenomenon appears as soon as the radius of gyration of the polymer is larger than the pore diameter. Using Poiseuille law it can be associated to a critical pressure P_c. We have shown that in this framework the frequency of translocation for any pressure difference P is given by:

$$f = k \frac{P}{P_c} \exp(-\frac{P_c}{P})$$

where k is a numerical factor determined by the geometry of the nanoporous membrane (pore density, homogeneity). Knowing the hydrodynamical resistance of the pore and the critical flow J_c it can be shown that: $P_c = 8 \cdot k_B T \cdot L / \pi R_{eff}^4$ with L the thickness of the nanoporous membrane. Combining with the previous expressions it follows that:

$$f = k(\frac{R_{eff}}{R_{pore}})^4 \frac{P}{P_c^0} \exp(-\frac{P_c^0}{P}(\frac{R_{pore}}{R_{eff}})^4)$$

With P_c^0 the critical pressure without polymer grafting i.e $R_{eff} = R_{pore}$.

A numerical solving procedure to determine the frequency of translocation is then achieved for each temperature and various values of w . The range of *w* and *v* values were chosen to be compatible with the literature (10). The other parameters were chosen as: R_0=2.5 nm, R_{pore}=25 nm, N=100, a=0.428 nm.

We observe in each case that the frequency of translocation as function of the temperature presents a sharp transition between no translocation at low temperature to full transmission at high temperature. The sharpness of the transition is dominated by the influence of the third virial coefficient w that is related to the chemical nature of the monomer (lateral groups).

S6: Molecular weight effect on critical pressure

We checked the dependence between $R_{eff,}$ the effective radius, and P_c, the critical pressure observed during translocation experiments, with a well-studied, flexible, and hydrophilic polymer (Polyethylene glycol terminated by a thiol function, PEG-thiol, with a molecular mass ranging from 356 Da to 20 kDa). Briefly, polymers were grafted onto the gold surface of the membrane at room temperature in presence of TCEP (5 mM) for 3h. After rinsing with buffer solution, the frequency of translocation was measured as a function of pressure. The resulting frequency versus pressure curves were fitted with the suction model and the critical pressure P_c was extracted for each grafting. The scaling of the radius of gyration of PEG with the molar mass is well established (11). and can be described as a polymer in good solvent. In each case, R_{eff} was thus determined from a scaling law $R_{eff}=R_{pore}$-a $N^{0.6}$ with a, the monomer size of PEG and N, the number of monomers. We observed a power law dependence of the critical pressure P_c with the effective radius (predicted as previously from an ideal coil model) with an exponent α=-3.9±0.2. This result, predicted by the suction model, confirms that when grafted with flexible and hydrophilic polymers the energy barrier of translocation through the pore is dominated by the entropic confinement of the DNA molecule.

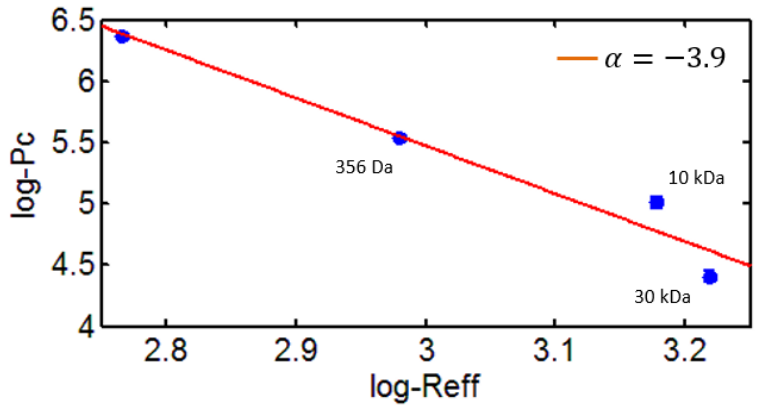

$$P_c = R_{hydro} J_c = k_B T \frac{8L}{\pi R^4}$$

$$P_c^{\exp} \propto R_{eff}^{-3.9\pm0.2}$$

Figure S6: Effect of polymer length on the critical pressure. The critical pressure for DNA translocation through PEG-grafted membrane is shown as a function of the effective radius R_{eff}.

S7 Discussion on thermophoresis, viscosity, and shear effects

In order to limit the number of possible interpretations of the observed phenomena we detailed here orders of magnitude of some additional phenomena:

Shear stress effects

Shear forces may impact the morphology of the grafted layer and shear may reduce the effective thickness of the grafted layer. Nevertheless, this effect will occur for speed flows which are much higher than the one of the present study. Indeed, as stated in (12), Weissenberg number Wi in the range of 0.1 to 1 would be necessary for this effect. In our system we can estimate $Wi=\gamma.\lambda$, with γ the shear rate and, λ the relaxation time of polymer. If we assume, that the shear rate is $\gamma=v/h$ (where v is the speed of the flow and h is the width of the speed gradient) and that the relaxation time is given by the Zimm time of the polymer, we obtain that: Wi = 0.01-0.02 in our system which are much smaller than the critical Weissenberg number necessary to induce conformational change of the grafted polymer.

Thermophoresis

The order of magnitude of thermophoresis impact can be estimated from previous studies. A modified Peclet number comparing thermal transport due to thermophoresis and thermal diffusion (13) is given by: $Pe(thermophor)=a\ S_T \nabla T$ where a is the size of the object i.e., the radius of gyration in the case of DNA, ∇T is the temperature gradient between the two compartment and S_T is the Soret coefficient a constant that have been already measured for DNA (14). In our case, with $\nabla T=10^6$ °C/m, a=0.8 µm and S_T~0.4, we obtain Pe(thermophor)~0.32. This demonstrates the small influence of thermophoresis compared to regular diffusion in our system.

Density and viscosity effects

We may assume that the effect of temperature on water would affect its viscosity and density. In the range of temperature where the critical transition is observed this would correspond to a change in viscosity of 13% and change in density of 0.2%. These changes would impact the

drag force on the polymer network and DNA by a similar factor. Such a small effect cannot be observed by our experimental design and would lead to a gradual increase of the translocation frequency for an increasing temperature whereas a sharp transition is observed in our work.

S8 Averaging effects on frequency versus pressure and frequency versus temperature curves

Frequency-pressure curves presented in the article (**Figure 4A, 4B**), were based on the averaging of data on different experiments. An example of the different individual experiments used for this averaging process is given below for 4 polymers: PMeOx (X_n=61, X_n=83) and P*n*PrOx (X_n=33, X_n=59).

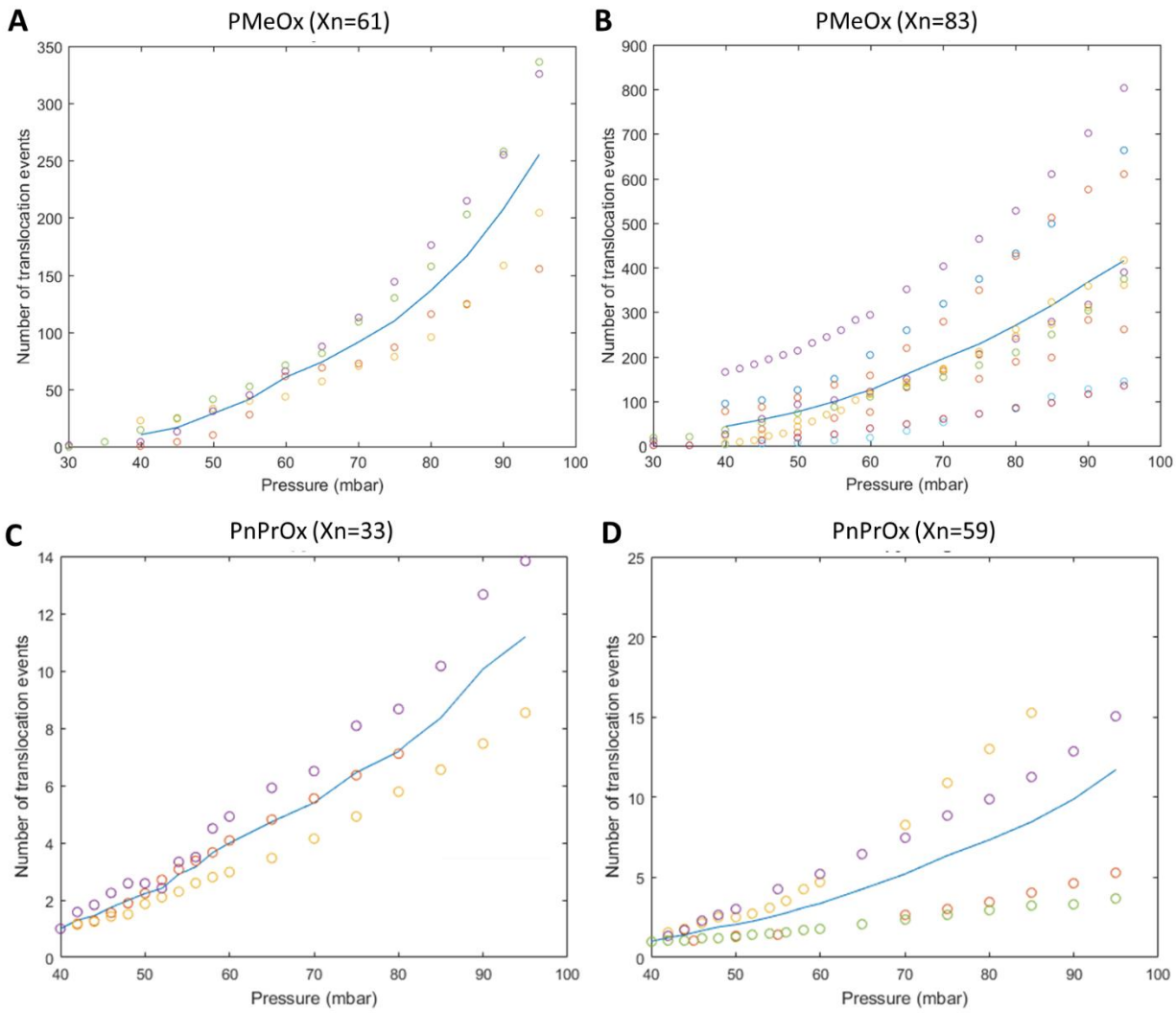

<u>Figure S8-1</u>: Unaveraged curves representing the normalized translocation frequency of *λ*-DNA as a function of pressure for different grafted pores: A) PMeOx (X_n=61), B) PMeOx (X_n=83), C) P*n*PrOx (X_n=33) and D) P*n*PrOx (X_n=59). For C) and D), the experiments were performed at high temperature (T=30 °C >LCST). The colors correspond to a different experiment based on the same grafted membranes. The blue curve represents the average. Pore diameter 42±0.5 nm.

Frequency-temperature curves presented in the article (**Figure 2B**), were based on the averaging of data on different experiments. An example of the different individual experiments used for this averaging process is given below for two polymers: P*n*PrOx (X_n=33) and P*n*PrOx (X_n=59).

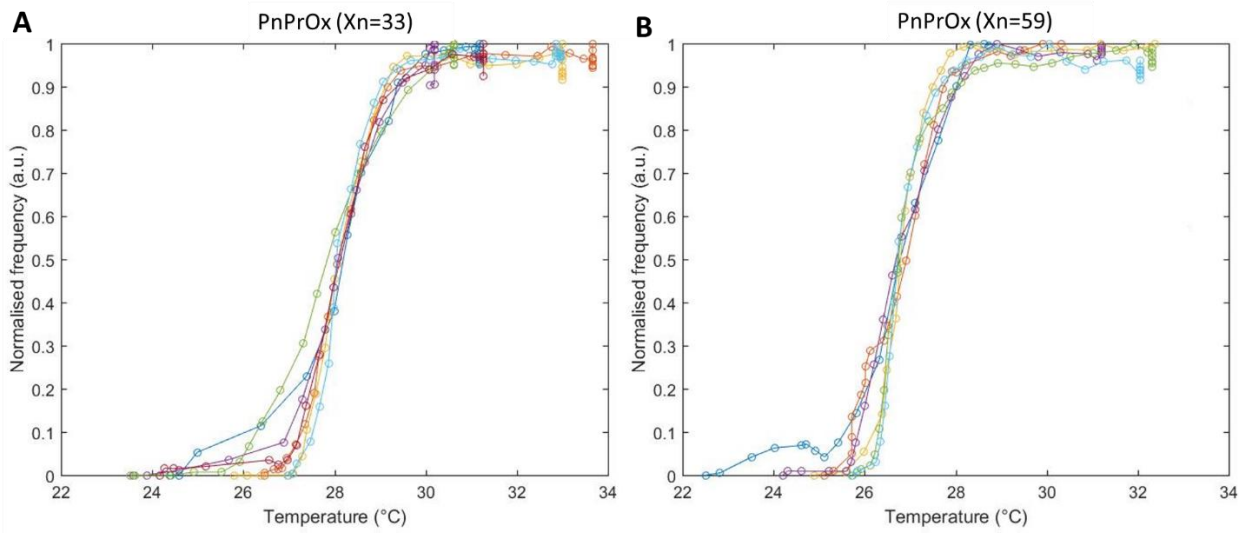

Figure S8-2: Unaveraged curves representing the normalized translocation frequency as a function of temperature for different grafted pores: A) P*n*PrOx (X_n=33) and B) P*n*PrOx (X_n=59). For A) and B) each color corresponds to a different experiment based on the same grafted membranes. Pore diameter 42±0.5 nm. Applied pressure: 80 mbar.

S9 SEM and AFM characterization of nanopores

Scanning Electron Microscopy, SEM

SEM images were performed to ensure that the gold deposition did not obstruct or alter the pore dimensions. Figure S9-1 shows a SEM image of a track-etched membrane after metallization, taken on the electron microscopy platform of the Condorcet building of Paris Diderot University. The membrane was broken by cryofracture (cooled at -80 °C and then fracture) to make the cross-sectional image. This can explain the distortions observed. The pores were not obstructed by the gold deposition, and they were cylindrical. The results from the measurement of the pore radius based on SEM images were shown in Table S9-1. The deviations from the nominal values are in agreement with those given by the manufacturer before gold deposition (*Whatman, GE Healthcare*).

Nominal diameter of the pore (nm) (+0%,-20%), given by the furnisher (Whatman, GE Healthcare) (before gold deposition)	Diameter measured by SEM (nm) (after gold deposition)
50	42±0.5
200	220±1.8

Table S9-1: **Pore diameters determined by SEM measurements**. Averaging over 200 pores.

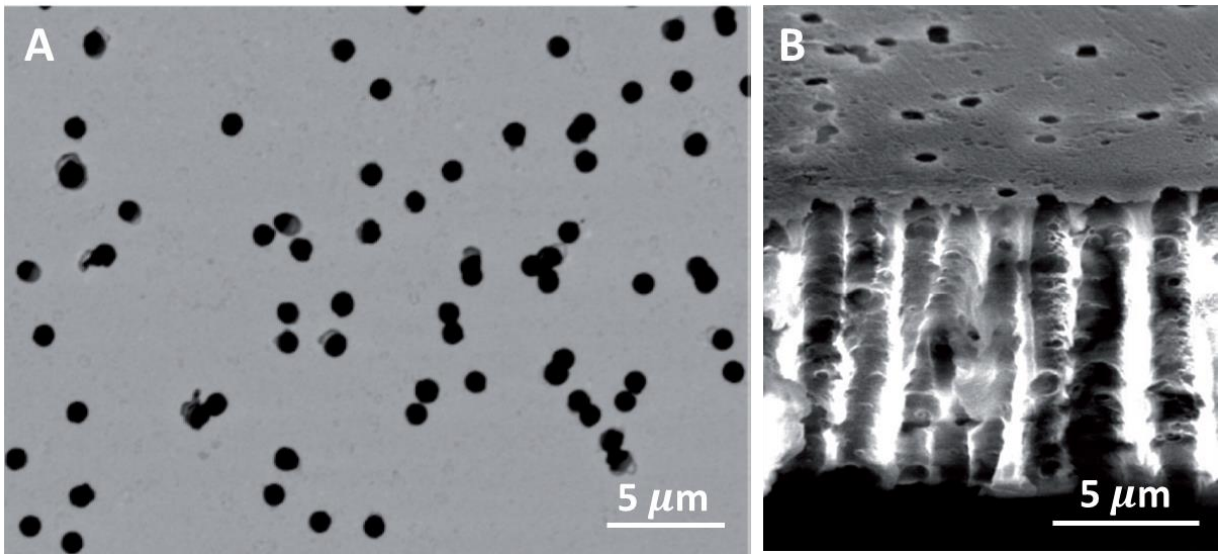

Figure S9-1: SEM images of 50 nm naked nanopores after gold deposition. A) Top view. B) Cross section view (made by cryofracture).

Atomic Force Microscopy (AFM) in liquid environment

To characterize the nanoporous membranes and polymer graftings, we used Atomic Force Microscopy (AFM). The AFM used was Bruker Nanoscope multimode 8 (scan E). In order to be in similar experimental conditions than during our nanopore experiments, we used peak force mode in liquid (tip Scan Asyst Fluid +, k=0.759 N/m). The different nanoporous membranes (naked or grafted) were sticked on a teflon ring with the help of a double-sided tape. The buffer used was Tris-EDTA (pH=7.5), as described in Material and Methods (Sample Preparation). For P*n*PrOx, tests were realized for a buffer temperature: T_{room}=23 °C. Because of the thermal heating of the membrane by the laser of the AFM system it is not possible to observe directly the process of opening and closing of the pores with this method.
The pore diameter was measured using the toolbox of Image J. Table S9-2 groups the values for the different data. Figure S9-2 to S9-4 are examples of AFM images for naked and grafted membranes (with PMeOx and P*n*PrOx). For both types of polymers, we observed that grafted nanopores exhibit a significantly smaller diameter than naked pores. Nevertheless, given the limited resolution of this measurement caused by both experimental and image analysis factors (non-flatness of the membrane, AFM tip dilation at the border of the pore) it was not possible to extract a precise measurement of the grafted layer in the pore. Beyond this limitation, this methodology validates the presence of polymer grafting in the nanopores.

	Naked (N=102)	Grafted PMeOx (X_n=387) (N=87)	Grafted P*n*PrOx (X_n=538) Room temperature (N=64)
Pore diameter (nm)	195 ± 19	145 ± 30	147 ± 18

Table S9-2: Pore diameters determined by AFM measurements. Averaging over N pores.

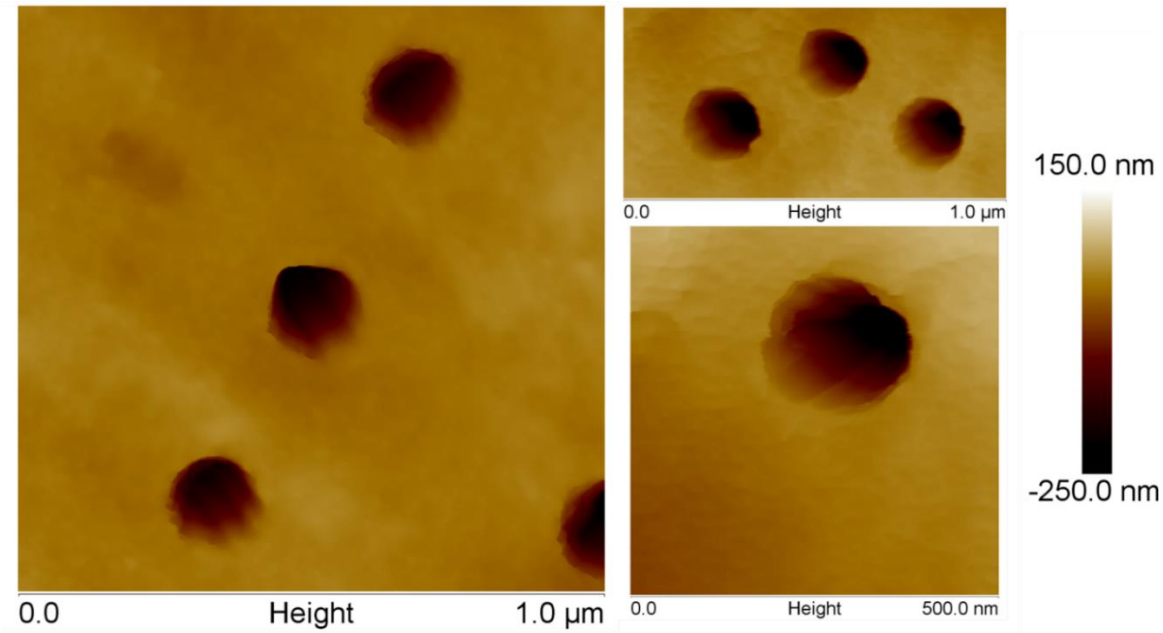

Figure S9-2: Typical AFM images of naked nanopores (polycarbonate covered with 50nm-thick layer of gold). Nominal pore diameter 200 nm.

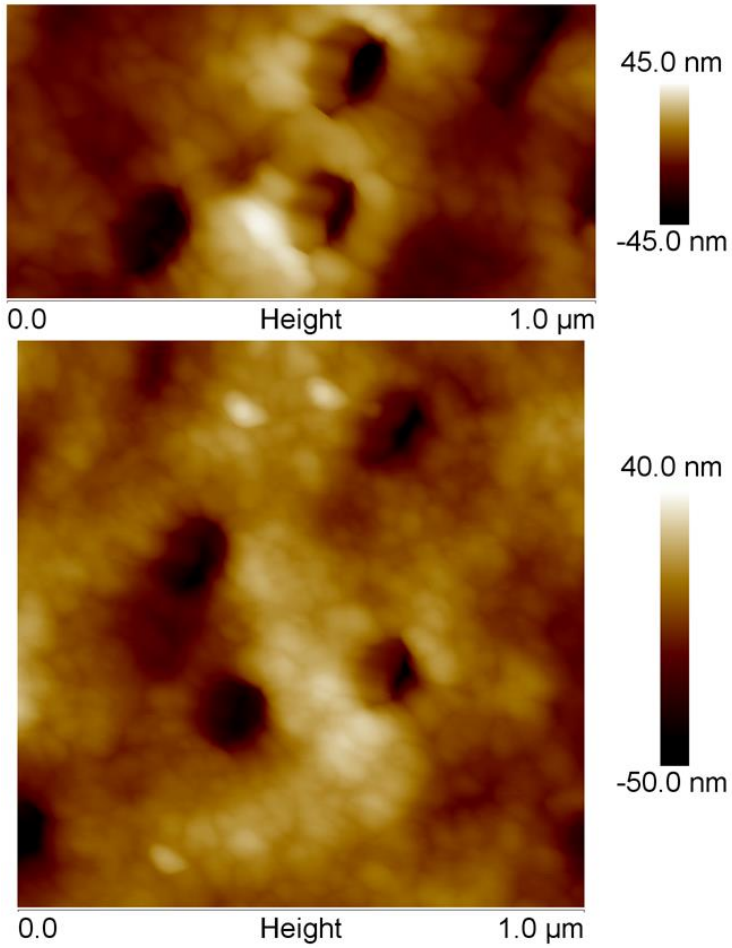

Figure S9-3: Typical AFM images of nanopores (polycarbonate covered with 50nm-thick layer of gold) grafted with PMeOx (X_n=387). Nominal naked pore diameter 200 nm**.**

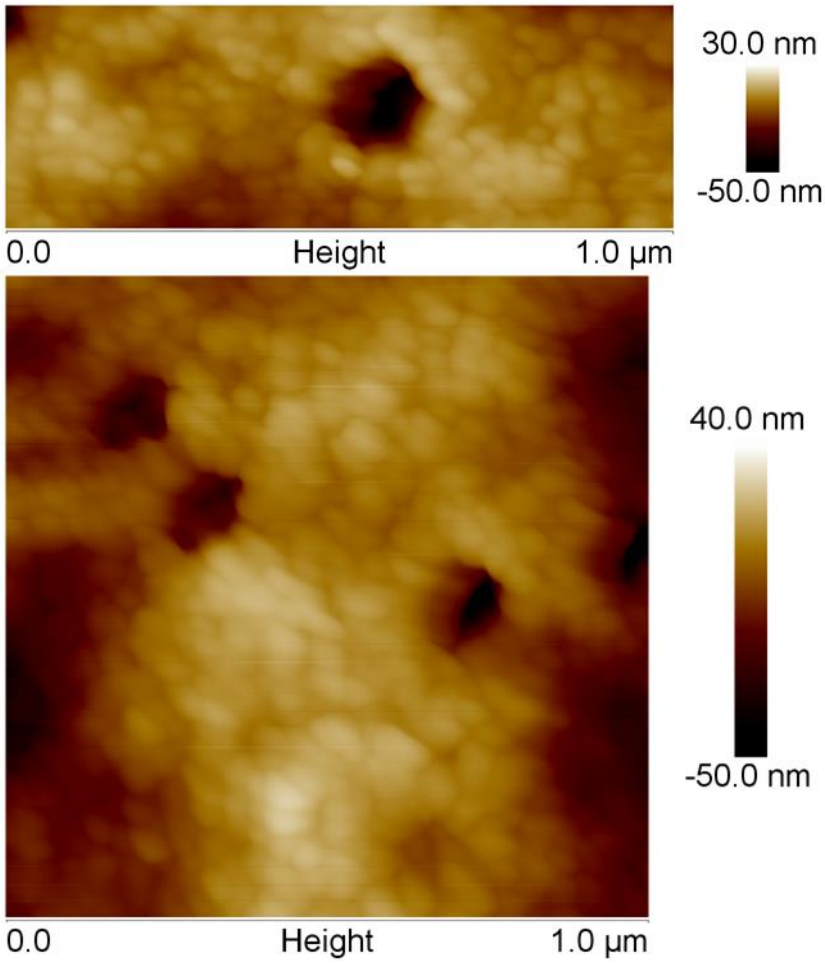

Figure S9-4: Typical AFM images of nanopores (polycarbonate covered with 50nm-thick layer of gold) grafted with P*n*PrOx (X_n=538). Nominal naked pores diameter 200 nm.

S10 Non normalized frequency temperature curves

Frequency-temperature curves presented in the article (**Figure 2B**), were based on the averaging of data on different experiments and then on the normalization of the frequency in order to be able to compare the curves between them and with the proposed model. Examples of raw data for different individual experiments are given below for the transport of both λ-DNA and viral capsids.

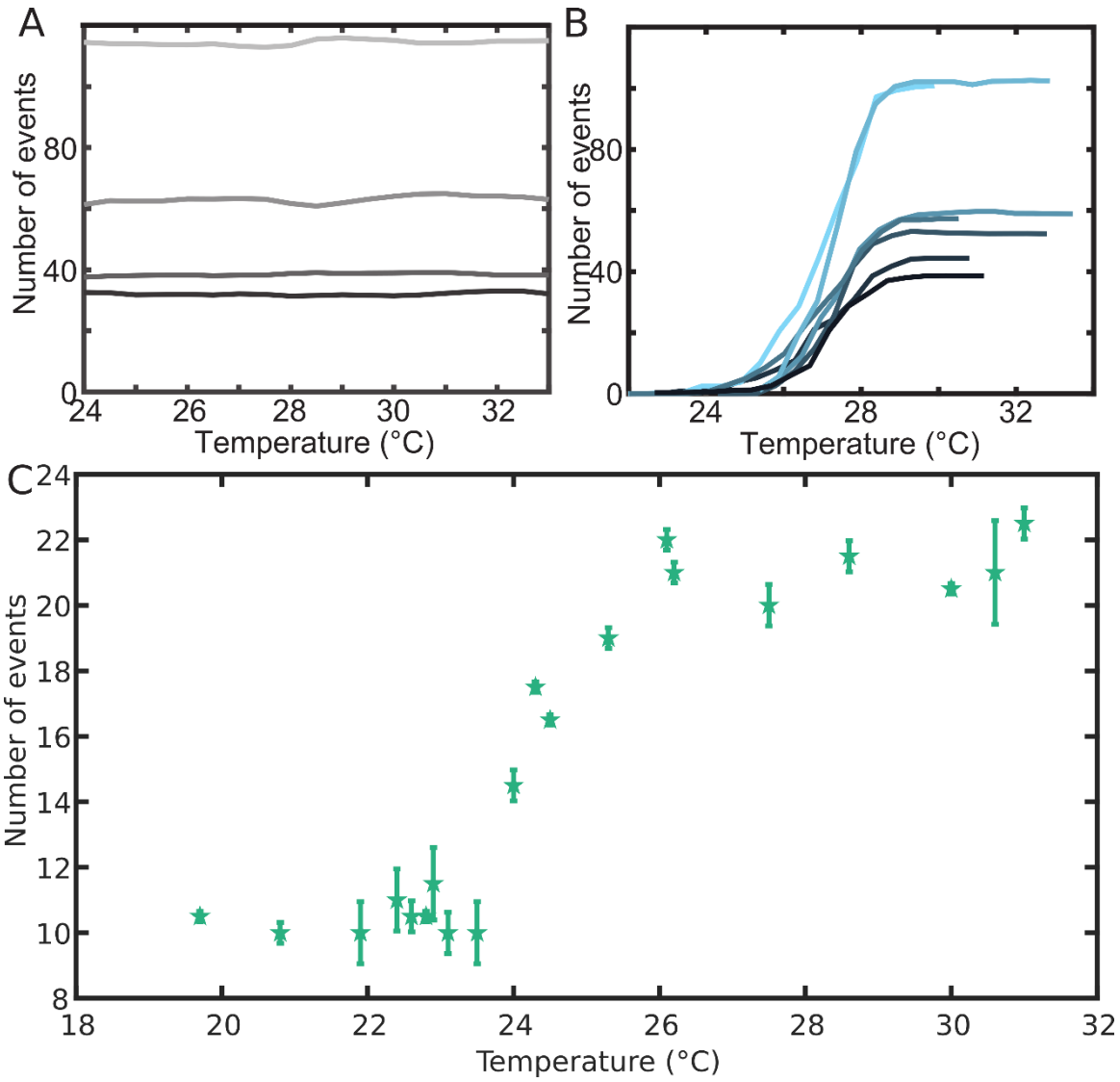

Figure S10: Non-normalized frequency temperature curves. Evolution of the number of events as a function of temperature. A) Translocation of λ-DNA trough a naked membrane (pore diameter (42±0.5) nm, applied pressure 80 mbar). B) Translocation of λ-DNA through a grafted membrane with P*n*PrOx (X_n=33) (pore diameter 42±0.5 nm, applied pressure 80 mbar). C) Translocation of AAV viral particles through a grafted membrane with P*n*PrOx (X_n=210) (pore diameter (220±1.8) nm, applied pressure: 4 mbar).

S11 Stability of the grafting

To test the stability of the grafting over time, we performed experiments on the same membrane with a time span of about 6 months. During this period, the membrane was stored in water at 4 °C. Typically, the membranes were used during a period of 2 to 4 months.

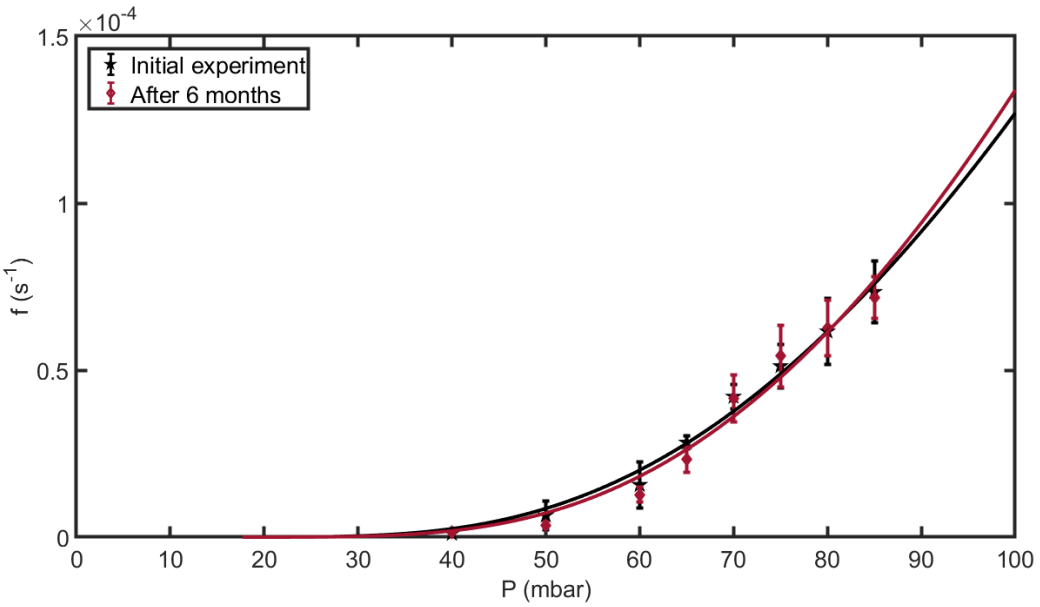

Figure S11: Stability test on grafting membrane. Evolution of the translocation frequency (f) as a function of the applied pressure (P) for λ-DNA through a membrane of 50 nm diameter nanopores and grafted with PMeOx (X_n=178). The experiment was performed at time zero after grafting of the membrane (initial experiment, in black) and after a period of 6 months (in red) during when the membrane was stored in water at 4 °C. The solid lines correspond to the suction model.

S12 Video example

Example of a video corresponding to the translocation of λ-DNA trough 50 nm pores grafted with PMeOx (Xn= 178). Applied pressure: 70 mbar. This is a raw video before any data analysis.

REFERENCES

1. Auger T, Bourhis E, Donnez J, Durnez A, Di Meglio JM, Auvray L, et al. Zero-mode waveguide detection of DNA translocation through FIB-organised arrays of engineered nanopores. Microelectronic Engineering. 2018;187-188:90-4.
2. Auger T, Mathé J, Viasnoff V, Charron G, Di Meglio J-M, Auvray L, et al. Zero-Mode Waveguide Detection of Flow-Driven DNA Translocation through Nanopores. Physical Review Letters. 2014;113(2):028302.
3. Bélanger D, Pinson J. Electrografting: a powerful method for surface modification. Chemical Society Reviews. 2011;40(7):3995-4048.
4. Stockhausen V, Nguyen VQ, Martin P, Lacroix JC. Bottom-Up Electrochemical Fabrication of Conjugated Ultrathin Layers with Tailored Switchable Properties. ACS Applied Materials & Interfaces. 2017;9(1):610-7.
5. Salvetti AO, S.; Chadeuf, G.; Favre, D.; Cherel, Y.; Champion-Arnaud, P., David-Ameline, J; and Moullier, P. Factors Influencing Recombinant Adeno-Associated Virus Production. Human Gene Therapy. 1998;9(5):695-706.

6. Delecourt G, Plet L, Bennevault V, Guégan P. Synthesis of Double Hydrophilic Block Copolymers Poly(2-oxazoline-b-ethylenimine) in a Two-Step Procedure. ACS Applied Polymer Materials. 2020;2(7):2696-705.
7. Plet L, Delecourt G, Hanafi M, Pantoustier N, Pembouong G, Midoux P, et al. Controlled star poly(2-oxazoline)s: Synthesis, characterization. European Polymer Journal. 2020;122:109323.
8. Halperin A. Collapse of grafted chains in poor solvents. J Phys France. 1988;49(3):547-50.
9. Gay C, de Gennes PG, Raphaël E, Brochard-Wyart F. Injection Threshold for a Statistically Branched Polymer inside a Nanopore. Macromolecules. 1996;29(26):8379-82.
10. Yamakawa H. Third Virial Coefficient of Polymer Solutions. The Journal of Chemical Physics. 1965;42(5):1764-71.
11. Linegar KL, Adeniran AE, Kostko AF, Anisimov MA. Hydrodynamic radius of polyethylene glycol in solution obtained by dynamic light scattering. Colloid Journal. 2010;72(2):279-81.
12. Biagi S, Rovigatti L, Abbasi M, Bureau L, Sciortino F, Misbah C. Hydrodynamic instability and flow reduction in polymer brush coated channels. Soft Matter. 2021;17(40):9235-45.
13. Reineck P, Wienken CJ, Braun D. Thermophoresis of single stranded DNA. ELECTROPHORESIS. 2010;31(2):279-86.
14. Duhr S, Arduini S, Braun D. Thermophoresis of DNA determined by microfluidic fluorescence. The European Physical Journal E. 2004;15(3):277-86.